ELSEVIER

Wear 220 (1998) 80–91

WEAR

Rolling contact fatigue performance of plasma sprayed coatings

R. Ahmed [a,*], M. Hadfield [b]

[a] Cambridge University, Department of Engineering, Trumpington Street, Cambridge, CB2 1PZ, UK

[b] Bournemouth University, Department of Product Design and Manufacture, Tribology Design Research Unit, Bournemouth, BH1 3NA, UK

Received 18 December 1997; accepted 1 May 1998

Abstract

This experimental study describes the Rolling Contact Fatigue (RCF) performance and the failure mechanisms of plasma sprayed tungsten carbide cobalt (WC–15%Co) coatings. The advancements of plasma spray coatings due to higher velocity and temperature of the impacting lamella call for investigations into new applications. One possible application is the rolling element bearing. A modified four ball machine which models the configuration of a deep groove rolling element ball bearing was used as an accelerated method to compare the rolling contact fatigue resistance of the test materials. RCF tests were conducted in conventional rolling element steel ball bearing (steel lower balls) and hybrid ceramic bearing (ceramic lower balls) contact configurations. Plasma sprayed coatings were deposited on a bearing steel (440-C) substrate at different thicknesses. The coated rolling element cones were ground and polished to achieve a good surface finish on the rolling elements. RCF tests were conducted under the various tribological conditions of contact stress, lubricant and test configurations. The frictional torque in the cup assembly was measured during the RCF tests with the aid of a force transducer. The speed of the planetary balls was monitored using an accelerometer and fast fourier transformation of the vibration signal. This enabled the experimental measurement of sliding between the coated cone and the driven balls. The failed rolling elements, coating debris and the lower planetary balls were analyzed for surface observations under the Scanning Electron Microscope (SEM), and Electro Probe Microscope Analysis (EPMA). The test results indicate that the coating performance was dependent upon the tribological conditions during the test. The failure modes were observed to be surface wear and the coating delamination. © 1998 Elsevier Science S.A. All rights reserved.

Keywords: Rolling contact fatigue; Plasma spraying; Coatings; Tungsten carbide; Wear debris

1. Introduction

The quest for improving the performance (higher load, speed, and low friction), and reliability (fatigue life) of rolling element bearings demands new approaches towards material selection and the optimization process. Overlay coatings, like thermal spraying, have the versatility of coating any material (provided it does not decompose during melting) on any substrate (if it can withstand coating temperatures), with the added advantage of high deposition rates and low production costs. It is possible that rolling element bearings can benefit from the advantages of high particle speed and temperature due to the developments in the thermal spraying processes. These coatings have already become an integral part of the aircraft and automobile industry [1]. The coating properties, like high hardness, and high resistance to the sliding and the abrasive wear specially in corrosive environments can be attractive to the rolling element bearing industry. However, the investigations on the fatigue performance of these coatings have been limited. Research is therefore required on the rolling contact fatigue performance and failure mechanisms of these coatings before consideration in the design of rolling element bearings. It may, therefore, be possible to reach the full potential of hybrid ceramic bearings and improve the performance of conventional steel bearings using the coated steel races. Other applications can include rolls for the rolling mills, crank and cam shaft and gear applications, etc.

Plasma spray coatings utilize the energy in a thermally ionized gas to melt and propel powder particles. These coatings are well known for there high particle temperatures during the spraying process due to the plasma jet which can be useful in spraying materials having high melting temperatures, e.g., ceramics, tungsten, etc. However, the particle speed in conventional air plasma spraying ranges from 150 m/s to 400 m/s in comparison to approximately 900 m/s for D-Gun (detonation gun) coatings. The low particle speed of the impacting lamella can result in a less dense and porous microstructure. Recent advancements in the air plasma spray coatings are geared towards a high velocity plasma spraying

* Corresponding author. E-mail: ra222@eng.cam.ac.uk.

0043-1648/98/$ - see front matter © 1998 Elsevier Science S.A. All rights reserved.
PII S0043-1648(98)00224-5

system. One of these advancements is the Gator–Gard system in which a particle speed of 1000 m/s has been achieved. These coatings have shown improvements in combating sliding wear of the components like bushings, flap tracks, fan blade mid spans, etc.

The complex lamella and anisotropic microstructure of plasma spray coatings means the analytical approaches to evaluate the fatigue resistance are expensive to solve. Hence, an experimental approach was adopted in which a modified four ball machine was used to investigate the performance of plasma sprayed rolling element cones. This study considers the rolling contact fatigue (RCF) performance of these coatings in various thicknesses subjected to various tribological conditions of contact configuration, contact stress, lubrication, and sliding in a rolling sliding contact.

The coating material was selected as WC–15%Co. Although this coating material deposited by D-Gun and HVOF processes is well known for its extremely high sliding and abrasive wear resistance, their is no significant data available on the performance of these coatings in pure rolling or rolling/sliding contacts. Further research is required to understand the performance and failure modes of these coatings deposited by thermal combustion spraying and thermal plasma spraying techniques in pure rolling or rolling/sliding conditions. Previous studies [3] by authors on WC–Co and Al_2O_3 coatings deposited by thermal combustion spraying process have indicated that WC–Co coatings not only performed better then Al_2O_3 coatings but also had a different failure mode. WC–Co coatings thus represents a combination of properties which can be useful in improving the RCF performance. It was the aim of this study to investigate the RCF performance of WC–15%Co coatings deposited by high velocity plasma spraying process. Other coating materials such as TiO_2, Cr_2O_3, WC–Ni–Cr, Al_2O_3 can also be investigated to broaden the spectrum of applications of thermal plasma spray coatings.

2. Coated cone rolling elements

Plasma sprayed tungsten carbide (WC–15%Co) coatings produced by Gator–Gard (GG102) system were deposited on the surface of a bearing steel (440-C) rolling element cones. The rolling element cones had a diameter of 15 mm and an apex angle of 109.4° or 90°. These rolling element cones were coated by spraying along the axis of the cone. The distance between the spraying gun and the rolling element cone was approximately 65 mm. The required coating thickness was obtained by several passes of the spraying gun perpendicular to the direction of spraying. The coating powder had a particle size of 10–25 μm. The substrate rolling element cones were machined from a bright finished 16 mm diameter bearing steel (440-C) rod. The substrate material was sand blasted and then preheated to approximately 100°C prior to the coating process for improved bonding at the interface by the mechanical interlock, increased surface area and reducing the quenching stresses of the impacting lamella.

The rolling element cones were sprayed to obtain an approximate coating thickness of 300 μm and 150 μm in the as-sprayed conditions. The cones were then ground and polished to give an average coating thickness of 230 ± 10 μm and 60 ± 10 μm for 109.4° apex angle cones and 150 ± 10 μm and 90 ± 10 μm for 90° apex angle cones. The average surface roughness of these rolling element cones in the as-sprayed, and polished conditions were 4.0 ± 1.5 μm (R_q), and 0.1 ± 0.05 μm (R_q) measured at a 0.8 mm cut-off length using a Gaussian roughness filter. These measurements were made in the direction perpendicular to rolling.

3. Test conditions and experimental test results

3.1. Modified four ball machine

A modified four ball machine shown as Fig. 1 was used to conduct the RCF tests of plasma sprayed coatings. The coated rolling element cone replaced the upper drive ball of the four ball assembly. The cup assembly for the test configuration was of type II [2] having a hardness of 60 HRC, whereas the steel planetary balls were grade 10 (ISO 3290-1975) carbon chromium steel with a hardness of 64 HRC and average surface roughness (R_a) of 0.02 μm. Two materials, i.e., bearing steel and silicon nitride ceramic, were used for the planetary balls. The steel lower balls were grade 10 (ISO 3290-1975) carbon chromium steel with an Ra of 0.02 μm

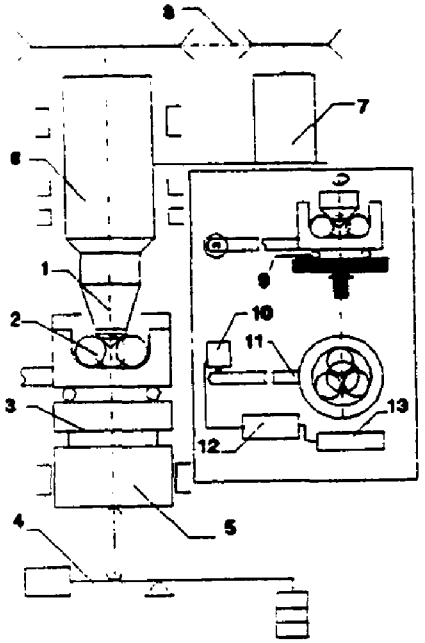

Fig. 1. Schematic of the modified four ball machine (1, coated cone and collet; 2, planetary balls; 3, heater; 4, loading lever; 5, loading piston; 6, spindle; 7, driving motor; 8, belt drive; 9, thrust bearing; 10, force transducer; 11, torque arm; 12, digital readout; 13, printer).

and hardness of 64 HRC. The R_a of the ceramic ball was 0.01 μm and ball roughness is within standard ball bearing tolerances. RCF tests were conducted at a spindle speed of 4000 ± 10 rpm and a contact load of 160 N on the contact surfaces. Experimental tests were conducted under immersed lubrication conditions using the high viscosity Hitec-174 lubricant and Exxon-2389 turbo lubricant. In addition to these lubricants, a test was also conducted in dry condition using air as a lubricant. The ratio (λ) of the fluid film thickness to the root mean square surface roughness (R_q) for the given test conditions can be approximately as $\lambda \geq 3$ and $\lambda \geq 1$ for the Hitec-174 and Exxon-2389 lubricant, respectively. The tests were conducted at an ambient temperature of 24 ± 2°C.

3.2. Frictional torque measurements

Fig. 1 also shows the schematic of the arrangement used to measure the total frictional torque in the modified four ball assembly. The arrangement consists of a torque arm protruding from the base of the cup assembly which contacts a force transducer at the other end in a horizontal plane. The transducer is calibrated before the measurements and measures the frictional force acting at the end of the lever arm. The output signal from the force transducer is sent to a digital display and then to a printer. The cup assembly rests on a rolling element thrust bearing. The frictional torque measured represents the sum of the frictional torque in the four ball cup assembly and the frictional torque due to the rolling element thrust bearing through which the load is applied to the cup assembly. The frictional torque values were recorded for the entire test duration and the averaged values are presented.

3.3. Ball kinematics

Fig. 2 shows the schematic of the arrangement used to monitor the ball kinematics within the cup assembly of the modified four ball machine under the given test conditions. A piezoelectric transducer (accelerometer) having a resonant frequency of 53 kHz was attached to the body of the cup assembly in the vertical plane. The vibration signal from the accelerometer was then amplified and fed into a signal processor where a fast fourier transformation (FFT) of the vibration signal was computed. This enabled the vibration amplitude to be measured in the frequency domain instead of the time domain. Hence, a precise measurement of the characteristic frequencies at which the driver and driven balls were rotating was made along with their amplitude of vibration. These frequencies which were representative of the angular velocity of the driver and driven balls were then used to calculate the surface speed of the driver (V_d) and the driven (V_p) balls. This enabled the investigation of the sliding within the contact region of the driver and the driven rolling element balls using the following equation:

$$\text{Sliding}(\%) = \{1 - (V_d/V_p)\} \times 100 \quad (1)$$

where V_d is the surface speed of the driver rolling element at the point of contact (m/s), and V_p is the surface speed of the driven rolling element at the point of contact (m/s).

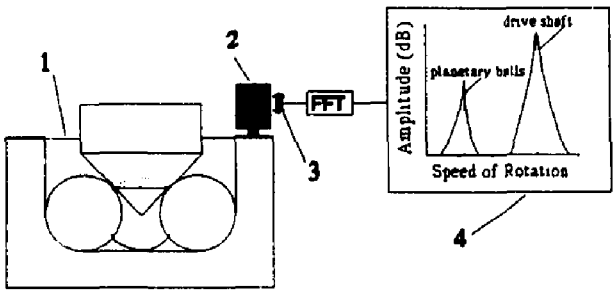

Fig. 2. Schematic of the ball orbital speed monitoring mechanism. (1, cup assembly; 2, accelerometer bolted to cup assembly; 3, vibration signal; 4, output).

3.4. Experimental test results

Table 1 summarises the experimental test results in terms of contact stress, test configuration and test duration. The results of average frictional torque, and percentage sliding have also been included. The contact stress and contact area described represent the calculations based upon the assumption of uncoated contact configuration. The test results are intended to be used to give an appreciation of the performance of the coated rolling element cones and are not intended to be used for the statistical fatigue life prediction.

4. Surface observations

4.1. Failed rolling element cones

Fig. 3 shows the surface observations of the 215 μm thick coated rolling element cone tested with steel lower balls subjected to the test GG1AX. Fig. 3a shows the overall view of the failed area. The coating failure initiated and propagated from within the coating microstructure which was confirmed by the EPMA analysis. Fig. 3b shows a portion of the wear track at a higher magnification. Numerous micropits are visible on the surface of the wear track and there depth was approximated as 5 μm (based on the surface observations at a higher magnification taken at an inclined angle to the surface). The width of the wear track is approximated as 700 μm and it can be appreciated that the width of the wear track is much greater than the contact dimensions of 132 μm (uncoated conditions) for the given test conditions. This indicates that the surface wear during the RCF test leads to the increased contact area. No delamination was observed in this case the micro-pits and the surface wear lead to the failure of the rolling element cone.

Fig. 4 shows the surface observations of the 215-μm thick coated rolling element cone tested with ceramic lower balls subjected to the RCF test GG2AX. Fig. 4a shows the overall view of the wear track. The rolling element failed from within

Table 1
Rolling contact fatigue test results for plasma sprayed coatings

Test no.	Average coating thickness (μm)	Lower balls	Contact stress[a] (GPa)	Contact width (mm) : b)	Depth of maximum shear (0.65 b) (μm)	Lubricant	Sliding (%)	Frictional torque (Nm)	Time to failure (min)
GG1AX	215	steel	2.74	0.132	85	Hitec 174	+2.3	0.0312	4290
GG2AX	215	ceramic	3.1	0.124	80	Hitec 174	+2.8	0.015	1099
GG3AX	260	steel	2.74	0.132	85	Exxon	+2.8	0.038	481
GG4AX	225	ceramic	3.1	0.124	80	Exxon	+2.8	0.003	99
GG5AX	260	steel	2.74	0.132	85	Dry	+0.3 to −9.6	0.06 to 0.175	99
GG1AY	60	steel	2.74	0.132	85	Exxon	+2.8	0.01	180
GG2AY	70	ceramic	3.1	0.124	80	Exxon	+0.3	0.03	49
GG3AY	60	ceramic	3.1	0.124	80	Hitec 174	+2.3	0.097	20
GG4AY	50	steel	2.74	0.132	85	Hitec 174	+0.3	0.05	518
GG1BX	140	ceramic	3.1	0.124	80	Hitec 174	−0.3	0.019	89
GG2BX	140	steel	2.74	0.132	85	Hitec 174	−3.25	0.04	450
GG3BX	140	ceramic	3.1	0.124	80	Exxon	−3.25	0.026	62
GG4BX	130	steel	2.74	0.132	85	Exxon	−0.3	0.01	123
GG1BY	90	ceramic	3.1	0.124	80	Exxon	−3.25	0.048	06
GG2BY	80	steel	2.74	0.132	85	Exxon	−3.25	0.036	90
GG3BY	90	ceramic	3.1	0.124	80	Hitec 174	−2.7	0.032	35
GG4BY	90	steel	2.74	0.132	85	Hitec 174	−2.7	0.033	90

[a]Uncoated case.

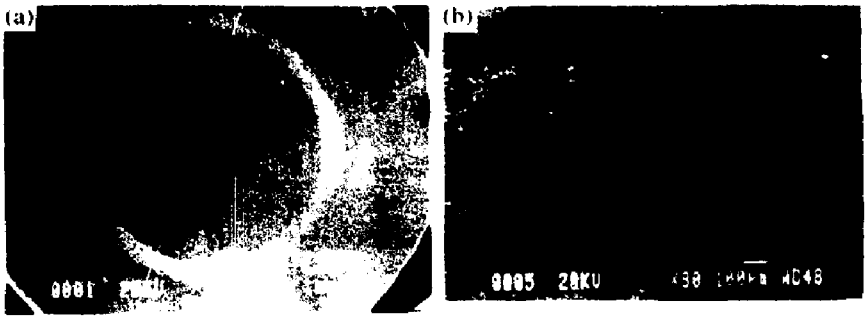

Fig. 3. Surface observations of the rolling element cone GG1AX; (a) Overall view (SEI); (b) Wear track (SEI).

Fig. 4. Surface observations of the rolling element cone GG2AX; (a) Overall view (SEI); (b) Wear track (SEI).

the coating microstructure and this was confirmed by EPMA analysis and BEI image. Fig. 4b shows a portion of the wear track at a higher magnification. The width of the wear track can be approximated as 450 μm. It can be appreciated that the width of the wear track in this case is smaller than what was seen in GG1AX which could be attributed to the contact with the lower ceramic balls (less contact width) and less duration of the test. A shallow pit of the approximate dimensions 300×300 μm can be seen in the middle of the wear track. It is possible that the tiny shallow pits combined with each other to form these bigger pits which eventually lead to the coating failure.

Fig. 5a shows the overall view of the failed area for the test GG4AX in BEI. The coating delaminated catastrophi-

Fig. 5. Surface observations of the rolling element cone GG4AX: (a) Overall view (BEI); (b) Wear track (SEI).

cally all the way around the wear track from within the coating microstructure. Fig. 5 shows a portion of the wear track at a higher magnification and numerous cracks can be seen on the surface of the wear track.

Fig. 6 shows the surface observations of the rolling element cone subjected to the test GG2AY. Fig. 6a shows the surface observations of the overall view of the wear track in SEI. In this case the coating delaminated at the coating substrate interface as was confirmed by the EPMA analysis and BEI images. Fig. 6b shows the delaminated coating at a higher magnification in BEI. The dark portions in this figure represent the substrate material (Fe). The rolling direction was from the left to the right of the figure. Fig. 6c shows the inclined angle view of the of the trailing edge of the wear track. Numerous cracks can be seen on the surface of the failed coating. The depth of delamination can be approximated as 40 μm. Fig. 6d shows a portion of the wear track at a higher magnification. Small and large pits can be seen on the surface of the wear track. The surface observations of the rolling element subjected to the test GG3AY were similar to the surface observations of GG2AY

Fig. 7 shows the surface observations of the 90-μm thick rolling element cone subjected to the test GG1BY. Fig. 7a shows the overall view of the wear track in BEI for the test GG1BY. In this case the coating delaminated from within the coating microstructure at some locations whereas the coating delaminated at the coating substrate interface as seen on the left hand side of the figure. Fig. 7b shows the interfacial delamination at a higher magnification. Fig. 7c shows the same area at an inclined angle and the depth of delamination can be appreciated as 100 μm approximately. Fig. 7d shows the inclined view at a higher magnification. Numerous cracks can be seen within the coating microstructure under the surface of the wear track.

Fig. 8 shows the surface observation of the rolling element cone tested under dry conditions (GG5AX). Fig. 8a shows the surface of the wear track in BEI. The coating failed under severe surface wear. Fig. 8b shows the surface of the wear

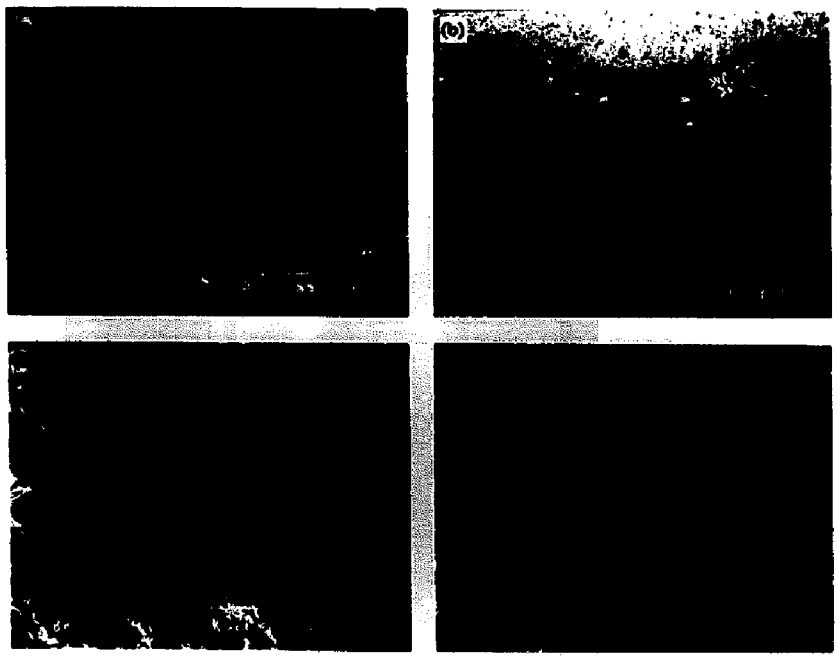

Fig. 6. Surface observations of the rolling elements GG2AY: (a) Overall view (SEI); (b) Delaminated coating (BEI); (c) Trailing edge (SEI); (d) Wear track (SEI).

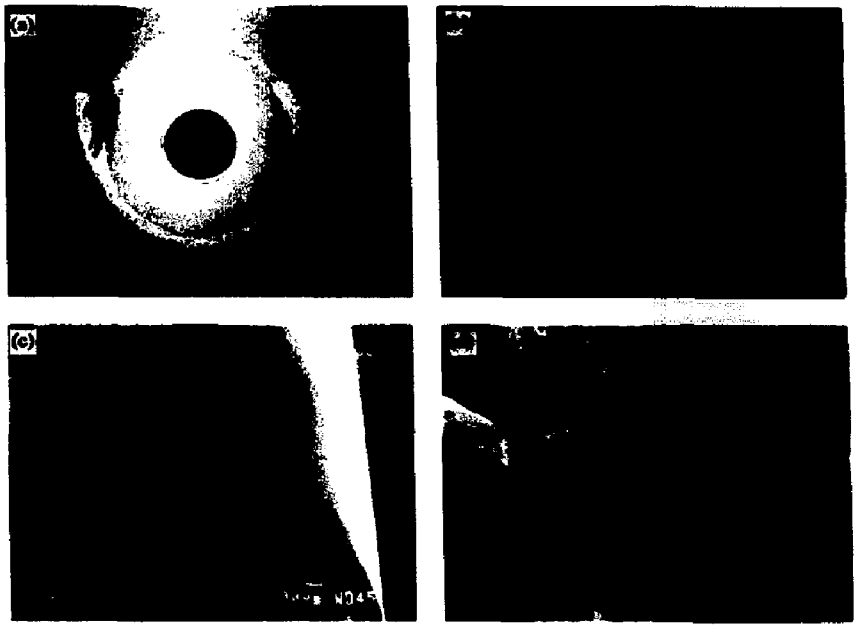

Fig. 7. Surface observations of the rolling elements GG1BY: (a) Overall view (BEI); (b) Coating delamination (SEI); (c) Inclined view (SEI); (d) Inclined view (SEI).

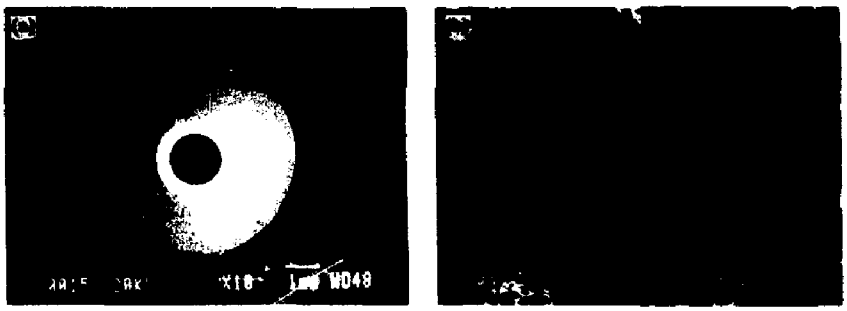

Fig. 8. Surface observations of the rolling element cone GG5AX; (a) Overall view (BEI); (b) Wear track (SEI).

track at a higher magnification. The depth of the wear track was approximated as 128 μm measured using the talysurf using a waviness filter at a cutoff of 0.8 mm.

4.2. Debris analysis

Fig. 9a shows the debris collected from the lubricant (Hitec-174) used for the test GG1AX. EPMA analysis of the debris showed a mixture of W, Co and Fe which indicated that the debris were generated from the coated rolling element cone as well as from the lower planetary balls. The size of these debris can be approximated as from 1×1 μm to 10×5 μm. Fig. 9b shows the debris collected from the debris test (GG5AX). The size of debris range from 1×1 μm to 20×5 μm. EPMA analyses of these debris show a combination of W, Co and Fe.

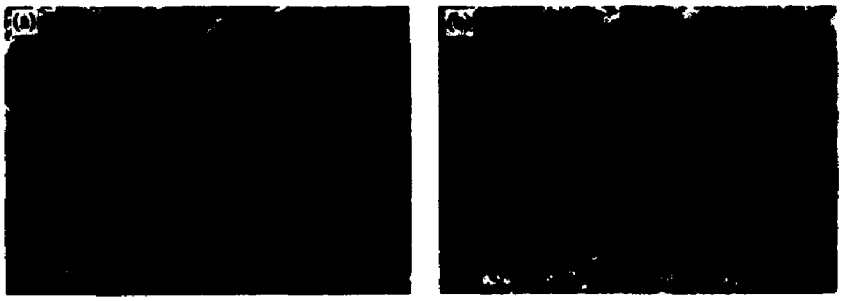

Fig. 9. Surface observations of the debris (GG1AX and GG5AX): (a) debris (SEI); (b) debris (SEI).

Fig. 10 shows the surface observations of the debris collected from the lubricant (Exxon-2389) used for the test GG4AX. Fig. 10a the top surface of the WC–Co debris. Fig. 10b shows the bottom surface of another debris collected from the lubricant an inclined angle. The thickness of debris can be approximated as 100 μm.

4.3. Surface analysis of the lower planetary balls

The lower planetary balls after the RCF tests were ultrasonically cleaned in acetone and dried before examining their surface in SEM. Fig. 11a shows the WC–Co debris observed on the surface of the ball for the test GG1AX, in BEI. The size of the debris can be approximated as 1×0.5 μm. Similar sized debris were observed on the surface of other planetary balls. Fig. 11b shows the surface observation of the wear track and many dents can be seen on the surface of the planetary ball at the location of the wear track.

Fig. 12a shows debris on the surface of the lower ceramic ball in BEI. The size of the debris can be appreciated as 5×3 μm and the EPMA analysis shows W and Co. However, debris on the surface of the lower ceramic balls was very rare. Fig. 12b shows the surface observation of the lower planetary balls used for the dry test (GG5AX) in BEI. The size of the debris can be appreciated as from 1×1 μm to 10×3 μm. These debris were confirmed to be W and Co by the EPMA analysis.

5. Discussion

The main objectives for this experimental study were to investigate the performance of plasma sprayed coatings during the RCF tests subjected to various tribological conditions and to classify the types of tribological failures on the basis of surface investigations. These features are then used to understand the main mechanisms which could have lead to these tribological failures. It should be appreciated that we are only concerned with the RCF performance of these coated

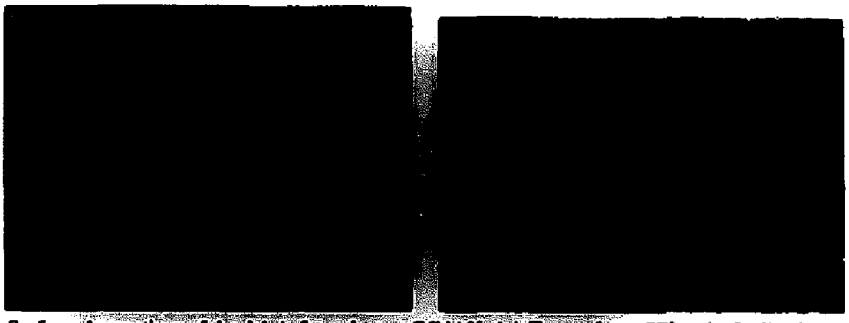

Fig. 10. Surface observations of the debris from the test GG4AX; (a) Top surface (SEI); (b) Inclined view (SEI).

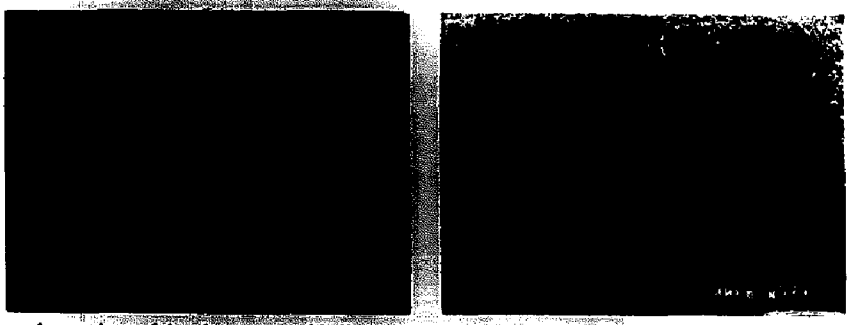

Fig. 11. Surface observations of the planetary steel balls (test GG1AX); (a) Debris (BEI); (b) Dents on the wear track (SEI).

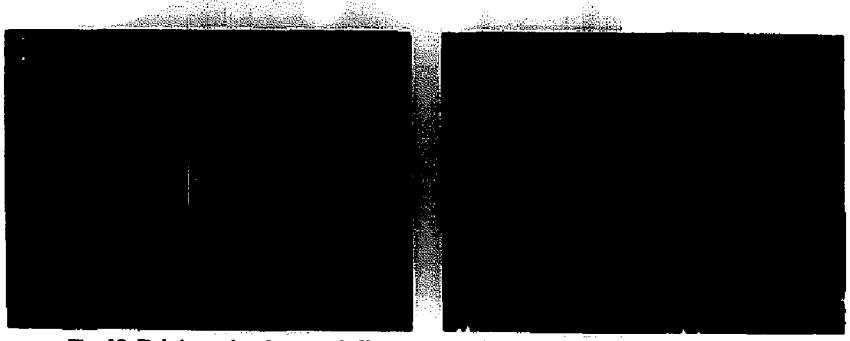

Fig. 12. Debris on the planetary balls; (a) Ceramic ball (BEI); (b) Steel ball (BEI).

rolling elements and the types of coating failures to provide a better understanding of the tribological behaviour of plasma sprayed coatings in rolling contact. The coating process parameters, coating powder e.t.c. used to spray the coatings were of conventional industrial practice which will not be discussed. Table 1 not only summarises the RCF performance of the coated rolling element cones but also defines the tribological conditions (parameters) varied during the RCF tests. It will be helpful to clearly explain these tribological parameters before appreciating their influence on the RCF performance of these coated rolling elements. It can be seen from Table 1 that four tribological parameters were varied in the testing programme. These parameters were as follows:

(a) The contact configuration, i.e., steel lower balls or ceramic lower balls to vary the contact area, contact stress, etc.

(b) The test lubricant to vary λ value from 1 to 3. All other changes due to variation in the test lubricant have been neglected.

(c) Coating thickness in the range of 60–220 μm.

(d) Gross sliding during the RCF tests caused by the differences in the apex angle of the rolling element cones.

The effect of these individual parameters on the RCF performance of the coated rolling element cones and the tribological mechanisms influencing the performance as discussed below.

5.1. Influence of contact configuration on RCF performance

The effect of contact configuration on the RCF performance can be seen by comparing the RCF tests conducted in conventional steel ball bearing and hybrid ceramic bearing configurations. As summarized in Table 1, it can be seen that in all the cases of RCF tests, the coated rolling elements performed better with steel lower balls then with the ceramic lower balls. This reduction in RCF life was approximately 25% to 50% when ceramic lower balls were used.

It can be appreciated that when the contact configuration was changed from conventional steel ball bearing (lower steel balls) to hybrid ceramic bearing (ceramic lower balls) not only the contact area was reduced but the Hertzian contact stress also increased from 2.7 GPa to 3.1 GPa (under the given test conditions). In the present analysis the contact load had to be increased by 50% (from 160 to 240 N) to increase the contact stress from 2.7 to 3.1 GPa for steel lower balls and visa versa. Similarly the contact load has to be decreased by 25% (from 160 to 120 N) to achieve the same contact area as was seen for ceramic lower balls. Both of these factors indicate severe tribological conditions leading to higher contact stresses when ceramic lower balls were used. This explains the reasons for the poor RCF performance (reduction of 25% to 50%) of the coated rolling elements when used in hybrid ceramic bearing configurations.

Apart from the changes in the contact width and Hertzian contact stresses other factors such as the hardness and wear resistance, e.t.c. of the planetary balls also becomes important when the lubrication conditions were in the mixed regime. This factor can be understood from the surface observations of the lower planetary balls which indicated, that except in one case (Fig. 12a) it was almost impossible to detect any debris on the surface of the lower ceramic balls. However, debris were seen in abundance on the surface of the lower steel balls. Similarly, dents were seen on the surface of lower steel balls but not on the surface of lower ceramic balls (Fig. 11b). The abrasion between the coated rolling element cone and lower balls with or without the presence of any wear debris damaged the lower steel balls resulting in dents but not with lower ceramic balls. Both of these observations indicate that the asperity behaviour changed when ceramic lower balls were used.

Although, it was not possible to confidently say if asperity adhesion was a phenomenon leading to the failure of rolling elements. If any such mechanism took place (adhesion of asperities) it effect was more pronounced with lower steel balls as more debris were seen on its surface. However, their is also a possibility that these debris were rolled between the cup and planetary balls and eventually embedded on the surface of planetary balls. Moreover, no ceramic debris were observed suspended in the test lubricants indicating that lower ceramic balls outclassed the coating much quickly due to their high wear resistance. This could mean harsh tribological conditions when ceramic lower balls were used due to its higher wear resistance and hardness in comparison to steel lower balls leading to quick failure.

Several researchers [4–6] have analytically and experimentally studied the behaviour of wear debris within the contact area of the bodies in rolling contact and indicated that the size, shape of debris along with other tribological conditions can effect this behaviour. In general, the mechanism of asperity contact in rolling sliding contact is complex depending upon the hardness, surface roughness, material, size and shape of debris, speed and lubricant behaviour. Any more discussion on debris behaviour is beyond the scope of this work. However, it is emphasised that it is not only the contact area and contact stresses which are effected by changing the planetary balls from steel to ceramic and visa versa but also the asperity contact in the rolling sliding contact for the tests in mixed lubrication conditions. Both of these factors contributed to the poor performance of these coatings when ceramic lower balls were used. However, When the lubricant film was fully developed ($\lambda \geq 3$), asperity behaviour can be ignored and only the contact area and stresses should be considered as influential factors effecting the RCF performance.

5.2. Influence of test lubricant on RCF performance

Two test lubricants were used in the testing programme. The effect of test lubricant on the lubrication regime, i.e., lambda (λ) value by varying the lubrication film thickness is considered here. As indicated in Section 3.1 this ratio (λ) was approximately 1 and 3 for the Exxon-2389 and Hitec-

174 lubricant, respectively. Considering the RCF test results (Table 1) it can be appreciated that in all the cases except the tests GG3AY and GG4BY, the coated rolling elements performed better with Hitec-174 lubricant than Exxon-2389. This was not only the trend for the RCF tests with lower steel balls but also for the lower ceramic balls. In most of the cases the RCF performance was reduced by approximately 65% to 90% when Exxon-2389 was used as the test lubricant. The reason for difference in the behaviour for the rolling element GG3AY might be due to high frictional torque (0.097 Nm) during that specific RCF test.

The above discussion on the behaviour of asperity contact (Section 5.1) with or without the presence of wear debris can also be used to explain the influence of lubrication regime on the performance of coated rolling elements. When Exxon-2389 ($\lambda \geq 1$) was used as test lubricant asperities must have come in contact, thereby accelerating the surface wear and increasing the frictional forces leading to quick failure of the rolling elements. Although, the difference seen in the frictional torque measurements when the test lubricant was changed was neither significant nor consistent, which could be due to these measurements representing frictional torque in the entire four ball cup assembly. Frictional torque measurements should therefore only be used for comparative studies and not for estimating the coefficient of friction. It should be noted that the readings presented in Table 1 indicate the steady state values. These values were comparable when the RCF tests were conducted with uncoated steel upper and lower balls which resulted in average values of 0.015 to 0.03 Nm. Surface observations of failed rolling elements indicated that surface wear was present for the tests conducted with both lubricants. This indicates that asperity contact was present with both the test lubricants. This could imply that the component of rolling friction caused by the asperity contact was present with both the lubricants. Hence no appreciable difference was observed in the values of frictional torque when the test lubricant was changed. It should also be appreciated that the frictional torque of 0.06 Nm at the start of dry test (GG5AX) in which asperity contact must have contributed substantially in the overall frictional torque was of the same order of magnitude as was generally observed with the lubricated tests (0.03 Nm). However, as the dry test continued the generation and presence of debris in the contact area significantly increased the frictional torque to 0.175 Nm. Thus the influence of wear debris on frictional torque measurements was more dominant then the asperity contact at the start of test.

The tests conducted with Hitec-174 lubricant thus performed better due to thick lubricant film which minimised the asperity contact and thus the wear and friction between the contacting rolling elements. The tests with Exxon-2389 as test lubricant had significant asperity contact which increased the surface wear and friction between the rolling elements leading to quick failure of coated rolling elements. The extent of asperity contact was further accelerated for Exxon-2389 lubricant due to the generation of wear debris.

5.3. Influence of coating thickness on RCF performance

Another parameter controlled during the testing programme was coating thickness. Two different coating thicknesses were used in each set of cones, i.e., the set of cones having 109.4° apex angle and 90° apex angle. These coatings can be broadly classified as thick coatings, i.e., (230 ± 10 and 150 ± 10 μm) and thinner coatings, i.e., (60 ± 10 and 90 ± 10 μm). This broad classification is based on the approximate depth of maximum shear stress under the given test conditions, i.e., the coating was thick if maximum shear stress was located within the coating microstructure and was regarded thinner if it was located at or below the coating substrate interface so that the effect of stresses at the coating substrate interface became important. It can be appreciated from Table 1, that thicker coatings performed better in all the cases of RCF tests in comparison to their thinner counterparts. Moreover, the reduction in RCF lifetimes when thinner coatings were used ranged from 50% to 90% with the exception of the test GG4BY in which case the reduction was less than 50%.

It can be appreciated from Table 1 that the depth of maximum shear stress ranges up to a depth of 90 μm under the surface of the wear track and its magnitude varied from 1 to 1.2 GPa under the given test conditions. This indicates that when thicker coatings were used the effect of applied load at the coating substrate interface became less important as majority of the shear stresses were located within the coating microstructure. The better performance of thicker coatings indicated that the shear resistance of the coating microstructure was better then the shear resistance at the coating substrate interface. This shows that the crack initiation and propagation due to shear stresses must be quicker at the coating substrate interface than from within the coating microstructure thereby reducing the RCF life of thinner coatings. This is because the coating substrate interface represents a mismatch of the properties of the coating and substrate material leading to stress concentrations. The strain experienced by the coating and substrate will vary depending upon their modulus of elasticity and Poisson's ratio. This difference in strain acts as a stress gradient at the interface leading to coating failure at the interface. This can also be confirmed by the finite element studies as indicated in the work of Ahmed and Hadfield [7,8], in which thinner coatings indicated a sharp stress gradient which leads to stress concentrations at the interface.

It should be appreciated that the only mechanisms by which the coating and substrate are bonded together is the mechanical interlock and compressive residual stresses due to the mismatch in the thermal expansions of the coating and substrate material (the possibility of any chemical bonding due to activation energy is contradictory in literature). Studies on the residual stress measurements of WC–Co coatings produced by a variety of different techniques explained in the previous studies by Ahmed and Hadfield [9] indicated that the compressive residual stress in the rolling elements can be several hundreds of Mega Pascals but not as high as 1 GPa.

The applied shear stress of approximately 1.2 GPa can thus prove extremely high at the coating substrate interface. Hence the advantage of compressive residual stress to resist the coating failure diminishes as the applied stress increases. Similarly, the quenching stresses will be higher at the coating substrate interface at low preheat temperatures due to quick cooling of the lamella leading to additional stress concentrations. It does not imply that the quenching stresses, micropores, micro-cracks and secondary phase particles which are generally present within the coating microstructure do not lead to stress concentrations within the microstructure. It took longer for the cracks to initiate and propagate from within the coating microstructure than at the coating substrate interface resulting in better performance of thicker coatings. However, the reason for poor performance of thinner coatings when the coating failure was not due to delamination but due to the surface wear is not clear at this stage. This can be thought of an effect of residual stress variations with the changes in coating thickness, and influence of changes in lubrication regime for the two lubricants.

5.4. Influence of sliding on RCF performance

The extent of gross sliding in the four ball assembly was another parameter controlled during the RCF tests. Before discussing any effect of this parameter it is important to clarify the sign convention used to represent gross sliding in Table 1. When the lower planetary balls were orbiting slower than their theoretical speed (calculated under frictionless and pure rolling conditions) a positive sign was used indicating that the coated rolling element was on the faster side of the rolling sliding contact. Similarly if due to the contact geometry in the four ball assembly the lower planetary balls were orbiting faster than their theoretically calculated speed, a negative sign was used to indicate the sliding direction thereby meaning that the coated rolling element was on the slower side of the rolling sliding contact. If this analogy is followed it can be appreciated that, when the coated rolling element was on the slower side of the rolling sliding contact, the RCF performance was significantly reduced. This reduction in performance ranged from 40% to 90% when the coated rolling element was on the slower side in the rolling/sliding contact with the exception of GG3AY which might be due to high frictional torque during that specific test as indicated earlier.

Hence, the direction of sliding also had a pronounced effect on the RCF performance of the coated rolling element cones. This is consistent with the work done by Sado and Yamamaota [10] and Tyfor and Beynon [11] for uncoated rolling elements and Yoshida et al. [12] and Nakajima and Mawatari [13] for the coated rolling elements. A comparison of the RCF test results during this study and previous studies by other researchers indicated that the direction of sliding significantly effected the performance in a rolling sliding contact regardless of the test machines, e.g., two roller type, three roller type or four ball machine and the effect can be observed for a homogenous materials as steels as well as for the coated rolling elements. All of these experimental studies suggest that the fatigue cracks propagate in the driven rolling element (negative sliding) and crack propagation was resisted on the driving rolling element. This is thought to be a function of the direction of load movement to the direction of traction as shown in Fig. 13. Previous studies have indicated that when the direction of traction was opposite to the direction of load movement which appeared in the driving part of the rolling sliding contact crack propagation was resisted and visa versa. Studies by Hills et al. [14] have shown some understanding of the stress state in the driving and driven components in which Von-Mises yield contours shift towards the surface to a greater area in the driven part thereby increasing the probability of crack propagation in the driven part. However, his studies on the basis of the maximum tensile stress indicated the opposite to the experimental observations. The actual case of sliding in the modified four ball system is however much more complex due to the presence of a spin component and no analytical studies were done to study the influence of this component during this experimental work.

5.5. Types of coating failures

Surface observations of the failed coated rolling elements indicated that the coating failures observed on the surface of coated rolling element cones can be classified in to two categories, i.e., surface wear, subsurface delamination. The rolling elements failed in either one of the above categories or a combination of two depending upon the tribological conditions prevailing during the RCF tests. Their was no consistent trend between the tribological conditions and the type of coating failure. Surface wear was a failure mechanism seen with both the lubricants in all the cases of the RCF tests. However, in some cases this type of failure was observed along with the delamination type of failure and in some cases this was the only mechanism of coating failure. Figs. 3 and 4 represent some of the cases in which surface wear was mainly responsible for the failure of rolling elements for the plasma sprayed coatings. In this type of failure a shallow wear track

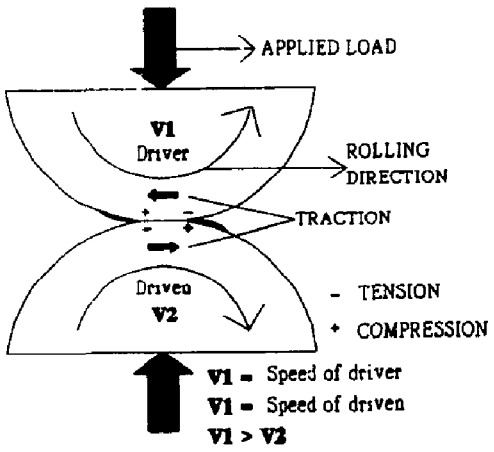

Fig. 13. Effect of traction in rolling sliding contact.

was formed the depth of which varied depending upon the contact configuration and the time to failure. As a result of this surface wear the contact became conforming and the width of wear track increased. Small wear debris of the type shown in Fig. 9a were produced during this type of failure. Small pits of the type shown in Fig. 3b were initially produced on the surface of the wear track. As the test continued these small and shallow pits joined together to form larger pits which lead to the failure of coated rolling element. A typical example of this behaviour can be seen from Fig. 4 in which these smaller and larger pits can be seen in the middle of the wear track. This type of failure was mainly due to the asperity contact, and due to the action of loose wear debris in the presence of gross sliding and microslip during the RCF tests.

Coating delamination was another type of failure seen on the surface of the rolling element cones. This type of failure was seen for the tests conducted with both the lubricants. Moreover, when the coated rolling element failed in delamination type failure the RCF performance was reduced. Figs. (5)–(7) show typical examples of this type of failure for the plasma sprayed coatings. In this type of failure larger debris of coatings delaminated parallel to the surface of the wear track resulting in sheet like debris as shown in Fig. 10. In the case of thinner coatings (coating thickness $< 100\ \mu m$) this type of failure generally took place at the coating substrate interface at an approximate depth of maximum shear stress (Fig. 6bFig. 7d). However in thicker coatings (coating thickness $> 150\ \mu m$) the delamination took place from within the coating microstructure (Fig. 5). The surface observations of the plasma sprayed coatings indicated that the depth of these failures can either be approximated as 40 micron or 90 μm under the given test conditions, which can be related to the depths of orthogonal shear stress or maximum shear stress, respectively. Small variations in the depth of failures from the calculated depths of shear stresses shown in Table 1 can be attributed to the assumption of the uncoated case. Previous studies by Ahmed and Hadfield [7,8] to evaluate the magnitude and location of stresses using finite element techniques have also shown that these depths can vary slightly from those calculated on the basis of uncoated case. However, even when the coatings delaminated at the depth of orthogonal shear stress or at the depth of maximum shear stress cracks at microscopic and macroscopic scale were visible at various depths under the surface of the wear track as shown in Fig. 6cFig. 7d which may have been caused by the stress concentrations due to the coating defects.

6. Conclusions

The RCF investigations of WC–15%Co coated rolling elements deposited by high velocity plasma spraying process indicated that the performance of these coatings is dependent upon the tribological conditions during the test. These tests were performed using a modified four ball machine and simulated the configuration of a deep groove rolling element ball bearing. Following conclusions summarise the outcomes of this investigation:

1. Thicker coatings performed better then thinner coatings which was mainly due to rapid crack initiation and propagation at the interface in thinner coatings.
2. RCF tests with high viscosity lubricant performed better then the tests with low viscosity lubricant which was mainly due to the effects of film thickness during the RCF tests.
3. RCF performed in conventional steel ball bearing configurations (steel lower balls) performed better then the tests performed in hybrid ceramic bearing configuration (lower ceramic balls) which was mainly due to severe tribological conditions during hybrid ceramic bearing configuration RCF tests.
4. The direction of sliding had a pronounced effect on the RCF life and the performance was reduced when the coated rolling element was on the slower side of the rolling sliding contact.
5. Two types of failures were observed from surface observations, i.e., coating wear and coating delamination. Their was no definite relation between the coating failure and tribological conditions during the RCF tests.

7. Abbreviations

BEI	Backscattered electron image
D-Gun	Detonation gun
EHL	Elasto-hydrodynamic lubrication
EPMA	Electron probe microscopy analysis
HVOF	High velocity oxy-fuel
RCF	Rolling contact fatigue
SEI	Scanning electron image
FFT	Fast fourier transformation

References

[1] Y. Arata, Thermal spraying—current status and future trends, ISBN 1241-3074, 1995.
[2] R. Tourret, E.P. Wright, Rolling Contact Fatigue: Performance Testing of Lubricants, Int. Symp., I. Petroleum, October 1976, Heyden & Son, London, ISBN 0 85501 301X, 1977.
[3] R. Ahmed, M. Hadfield, Rolling contact fatigue performance of detonation gun coated elements, Tribol Int. 30 (2) (1997) 129–137.
[4] K.K. Chao, C.S. Saba, P.W. Centers, Effects of lubricant borne solid debris in rolling surface contacts, Tribol. Trans. 39 (1) (1996) 13–22.
[5] R.S. Sayles, Debris and roughness in machine element contacts: some current and future engineering implications, J. Eng. Tribol. 209 (3) (1995) 149–172.
[6] K.N. Goddard, B.D. MacIsaac, Use of oil borne debris as a failure criterion for rolling element bearings, Lubric. Eng. 51 (6) (1995) 481–487.
[7] R. Ahmed, M. Hadfield, Rolling contact fatigue behaviour of ther-

mally sprayed rolling elements, Surf. Coatings Technol. 82 (1996) 176–186.
[8] R. Ahmed, M. Hadfield, Fatigue behaviour of HVOF coated M-50 steel rolling elements, J. Mater. Manuf. Processes, Special issue on thermal spraying, in print.
[9] R. Ahmed, M. Hadfield, Experimental measurement of residual stress field within thermally sprayed rolling elements, Wear 209 (1997) 84–95.
[10] N. Sado, T. Yamamaota, Effect of tangential traction and roughness on crack initiation/propagation during rolling contact, ASLE Trans. 25 (2) (1981) 198–204.
[11] W.R. Tyfor, J.H. Beynon, The effect of rolling direction reversal on fatigue crack morphology and propagation, Tribol. Int. 27 (4) (1994) 273–282.
[12] M. Yoshida, K. Tani, A. Nakahira, T. Mawatari, Conference Proceedings, International Thermal Spray Conference, Kobe, Japan, 663–668, ISBN 1-86058-1099, 1995.
[13] A. Nakajima, T. Mawatari, Surface durability of thermally sprayed WC cermet coating in lubricated rolling/sliding contact, World Tribology Congress, 1997.
[14] D.A. Hills, A. Sackfield, A.R. Uzel, Stress concentrations in tractive rolling Paper VII(ii), Leeds Lyon Symposium on Tribology, 171–178, 1985.

Biographies

Rehan Ahmed, BEng (Hons), MSc, PhD, AMIMechE, is a Research Associate at the Department of Engineering, Cambridge University. He is currently involved in a project related to the tribological modelling in roll bite during cold rolling. This project involves close collaboration with British Steel and Avesta Sheffield. Thin films such as roll transfer films, surface characterisation using interferometry, and mathematical modelling are the key features of the project. After completing his BEng (Honours) in 1992 he worked as an Engineer at ASIACON Private on a project with F.L. Smith of Denmark. He went back to academic education in 1993 to finish his MSc at the Brunel University. During his MSc dissertation he worked on applications of coatings for the industry. At this stage he developed interest in tribology of coatings and its applications. He stayed at the Brunel University to finish his PhD in fatigue failures of coatings. He then worked as a Research Associate on the design of oil-free compressors to reduce noise emissions. This project was sponsored by Devilbiss Health care, which is a division of Sunrise Medical. Rehan Ahmed has authored and co-authored numerous scientific publications. His specific interests of research are tribology of thick and thin coatings, residual stresses and surface characterisation using three-dimensional parameters.

Mark Hadfield, BEng (Hons), PhD, CEng, MIMechE, is a senior lecturer in the Department of Product Design and Manufacture at Bournemouth University. His career began by completing a 4-year officer cadetship with the Royal Fleet Auxiliary and serving as a sea-going marine engineer for another 4 years. He then commenced a degree in Mechanical Engineering at Brunel University. During his academic studies he worked for Marchant Filer Dixon (consulting engineers) and the Royal Aerospace Establishment (Farnborough). After graduation he worked for AE Piston Products as Senior Project Engineer. After this he completed his PhD in ceramic tribology with SKF Engineering and Research Centre (The Netherlands) and Brunel University (UK). Subsequently he was employed as a lecturer at Brunel University for 5 years before joining Bournemouth University in 1997. His research interests include tribology design and rolling contact fatigue of ceramics and coatings.